A 3D-Printed Electrical Impedance Tomography Tactile Sensor for Scalable Coverage

Haofeng Chen[1], Carson Kohlbrenner[2], Jiri Kubik[1], Lukas Rustler[1], Alexander Dickhans[2], Alessandro Roncone[2], Hyosang Lee[3], and Matej Hoffmann[1]

***Abstract*— Electrical impedance tomography (EIT) tactile sensors can detect pressure over continuous surface domains with sub-fingertip level resolution. However, state-of-the-art EIT tactile sensors are challenging to scale to large-area coverage of a robot without complete redesign of each unit due to complexities in the underlying shape of the target robot. In this work, we present an EIT tactile sensor with a unified fabrication process that does not depend on the target robot's shape by using multi-material 3D printing. Our sensors are composed mostly of 3D printed materials, eliminating the need to hand-tailor components. We demonstrate our approach by printing a curved U-shaped EIT sensor that achieved an average localization accuracy of 6 ± 4 mm when probed.**

I. Introduction

Tactile sensors that can mimic the biological sense of touch in robots are enabling for robots to safely and effectively interact with the physical environment [1]. Many solutions use modular taxels to scale to the robot's morphology [2], [3], but electrical impedance tomography (EIT) tactile sensors have been demonstrated as an emerging alternative due to their ability to sense over continuous domains with high resolution [4], [5]. The demand for whole-body coverage has kept pace with the improving capabilities of EIT sensors, and recent works have presented large-area instances of EIT sensors [6]–[8]. However, current EIT tactile sensors remain difficult to scale in practice because each instance is manually tailored for a robot's link, requiring a complete redesign for new surfaces.

3D printed tactile sensors have been demonstrated to be scalable to full body coverage when instances are designed to the target robot's morphology [9], [10]. Recent works have achieved EIT sensing over small surface areas using 3D printed components [4], [11], [12], but their fabrication requires many hand-tailored elements such as custom silicone molding. To unlock the large-area coverage benefits of 3D-printed tactile sensors such as form-fitting design and shape-agnostic fabrication, all structural components of the EIT sensor should be 3D-printable.

In this work, we present a 3D printed EIT tactile sensing platform that uses solely 3D-printed structural components, including the base; conductive layer; and external covering, to enhance large-area coverage robot surfaces. Our approach uses multi-material 3D printing to fabricate the conductive, flexible, and rigid elements.

The authors are at the [1]Humanoid and Cognitive Robotics group at CTU in Prague {first.last@fel.cvut.cz}, [2] Human Interaction and Robotics group at CU Boulder {first.last@colorado.edu}, and [3]Eindhoven University of Technology. This work is partially supported by European Union under the project Robotics and Advanced Industrial Production (reg. no. CZ.02.01.01/00/22_008/0004590) and NSF FW-HTF-R grant #2222952.

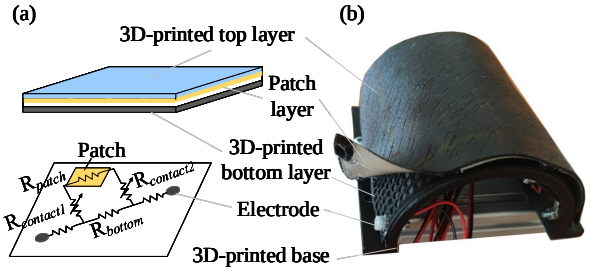

Fig. 1: The presented EIT sensor is comprised mostly of 3D-printed layers. Touch is localized when the patch layer comes into contact with the conductive bottom layer and changes the resistance between electrodes across the sensing domain.

II. Methods

A. Sensor Design and Fabrication

The proposed sensor adopts a multi-layer architecture as illustrated in Fig. 1. The U-shaped substrate has a radius of 40 mm and a length of 100 mm. The sensing structure consists of three primary layers: a 3D-printed conductive TPU bottom layer serving as the bulk conductor, a highly conductive patch layer that modulates local conductivity under mechanical contact, and a flexible 3D-printed top layer providing structural protection from collisions. Conductive features (sensing layer) used Recreus Conductive Filaflex TPU [13] and the top layers used Filaflex 60A TPU [14]. The patch layer currently uses conductive tape as the piezoresistive element, which can be replaced with high-conductivity 3D-printed materials for fully integrated fabrication. The assembly is mounted on a rigid 3D-printed base fabricated from PETG, which provides mechanical stability.

Sixteen electrodes are mounted on a 3D-printed base and arranged in a 4×4 grid along the curved surface, enabling EIT current injection and voltage measurement, which results in 120 measurements. The electrical behaviour of each sensing patch is captured by the equivalent circuit model shown in Fig. 1(a). Under surface normal loading, mechanical deformation of the patch increases the contact area between the patch and the bottom layer, reducing R_{patch} and locally increasing the resultant conductivity. This conductivity perturbation is detected by the EIT measurement system as a change in the boundary voltage pattern, which is then used to reconstruct the spatial distribution of conductivity change across the sensor surface.

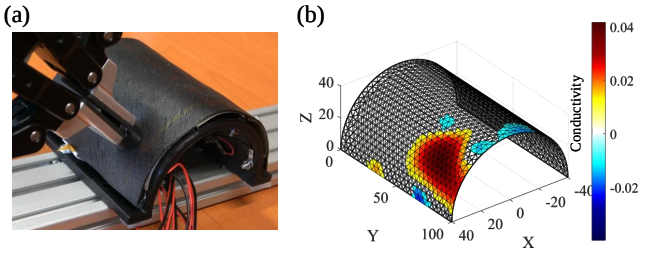

Fig. 2: Experimental validation. (a) Photograph of the indentation test setup. (b) Representative EIT reconstruction showing the localised conductivity change under single-point contact.

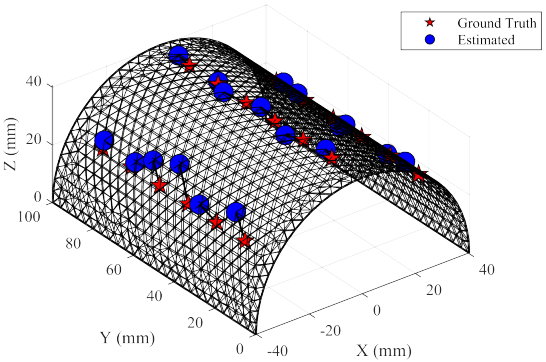

Fig. 3: Spatial distribution of ground truth and estimated contact positions on the sensor surface.

B. Inverse Reconstruction

Following the one-step Gauss–Newton formulation [15], the conductivity change is recovered in closed form as

$$\Delta\boldsymbol{\sigma} = \underbrace{(\mathbf{J}^T\mathbf{W}\mathbf{J} + \lambda^2\mathbf{R})^{-1}\mathbf{J}^T\mathbf{W}}_{\mathbf{RM}}\,\Delta\mathbf{V} \tag{1}$$

where $\mathbf{J} \in \mathbb{R}^{m\times n}$ is the sensitivity matrix relating boundary voltage changes $\Delta\mathbf{V} \in \mathbb{R}^m$ to conductivity changes $\Delta\boldsymbol{\sigma} \in \mathbb{R}^n$, $\mathbf{W}$ is a weighting matrix, λ is a regularization hyperparameter, and $\mathbf{R}$ is computed using the Laplace prior [16]. The reconstruction matrix $\mathbf{RM}$ is precomputed offline, enabling real-time tactile reconstruction at deployment.

III. Results and Discussion

A. Experimental Setup

A total of 18 predefined test indentations were arranged in a 6×3 grid on the curved surface to evaluate the sensor's localization performance. At each position, the indenter was held stationary for approximately five consecutive frames. Raw voltage measurements were stored as differential signals relative to a background reference $\mathbf{v}_h$ acquired at the start of each session. Press events were detected automatically using a per-channel normalized signal with rolling minimum baseline subtraction, followed by level-crossing onset detection. This approach accounts for the non-uniform sensitivity distribution inherent to EIT, which causes positions near the electrode boundary to produce significantly larger voltage responses than interior positions under equivalent loading. For each detected event, five consecutive frames centered on the peak response frame were extracted and averaged to produce a single representative voltage vector per position, suppressing frame-to-frame measurement noise.

Conductivity reconstructions were performed offline using the EIDORS toolbox [16] with a Gauss-Newton one-step solver and Laplace prior regularization (hyperparameter $\lambda = 0.1$). The forward model was defined on a tetrahedral finite element mesh comprising 5,714 elements. A representative reconstruction is shown in Fig. 2(b), where the contact region is clearly localized as a concentrated high-conductivity hotspot on the curved sensor surface.

B. Localization Error

The estimated contact location $\hat{\mathbf{p}}_r$ was computed as the weighted center of mass of finite elements exceeding 50% of the peak reconstructed conductivity change:

$$\hat{\mathbf{p}}_r = \frac{\sum_{i\in\mathcal{S}} \delta\sigma_i\, V_i\, \mathbf{c}_i}{\sum_{i\in\mathcal{S}} \delta\sigma_i\, V_i} \tag{2}$$

where $\delta\sigma_i$, V_i, and $\mathbf{c}_i$ denote the reconstructed conductivity change, volume, and centroid of the i-th element, and $\mathcal{S} = \{i : \delta\sigma_i > 0.5 \cdot \max_j(\delta\sigma_j)\}$ is the active element set. The estimate was subsequently projected onto the nearest surface mesh node to ensure the result lies on the physical sensor surface. The localization error PE_r was defined as the Euclidean distance between the projected estimate and the ground truth position $\mathbf{p}_r^{\mathrm{gt}}$:

$$\mathrm{PE}_r = \|\hat{\mathbf{p}}_r^{\mathrm{surf}} - \mathbf{p}_r^{\mathrm{gt}}\|_2 \tag{3}$$

The system achieved a mean localization error of 6.25 ± 3.55 mm across all 18 test positions, with a minimum of 1.54 mm and a maximum of 14.42 mm. Positions along the top arc column ($X \approx 0$ mm) and the right arc column ($X \approx +33$ mm) demonstrated consistently low errors, while positions in the lower rows of the left arc column exhibited higher errors, attributable to the combined effect of reduced boundary sensitivity and manual pressing uncertainty of approximately 8–12 mm observed in that region.

IV. Conclusion

This work introduces an EIT-based tactile sensor that is comprised of 3D-printed layers, bypassing the need for hand-tailored components. The experimental results show the tactile sensor achieved contact localization on a curved 3D surface with a mean absolute error of 6.25 mm, corresponding to 6.25% of the sensor length. This performance is achieved using a one-step Gauss-Newton reconstruction without any data-driven post-processing, exhibiting the practicality of 3D-printed EIT tactile sensing.

Future steps include using procedural design to generate complex form factors that are flush-fit with a target robot's surface [9], as well as 3D-printing the remaining non-structural components such as the electrodes and wires so that all components can be printed in a single print job [10].

REFERENCES

[1] C. Chen, Z. Yu, H. Choi, M. Cutkosky, and J. Bohg, "Dexforce: Extracting force-informed actions from kinesthetic demonstrations for dexterous manipulation," *IEEE Robotics and Automation Letters*, vol. 10, no. 6, pp. 6416–6423, 2025.

[2] G. Cheng, E. Dean-Leon, F. Bergner, J. R. G. Olvera, Q. Leboutet, and P. Mittendorfer, "A comprehensive realization of robot skin: Sensors, sensing, control, and applications," *Proceedings of the IEEE*, vol. 107, no. 10, pp. 2034–2051, 2019.

[3] Y. Zhou, J. Zhao, P. Lu, Z. Wang, and B. He, "Tacsuit: A wearable large-area, bioinspired multimodal tactile skin for collaborative robots," *IEEE Transactions on Industrial Electronics*, vol. 71, no. 2, pp. 1708–1717, 2023.

[4] H. Park, W. Kim, S. Jeon, Y. Na, and J. Kim, "Graph-structured super-resolution for geometry-generalized tomographic tactile sensing: Application to humanoid faces," *IEEE Transactions on Robotics*, vol. 41, pp. 558–572, 2024.

[5] M. Yang, "A biomimetic elastomeric robot skin using electrical impedance and acoustic tomography for tactile sensing," *Science Robotics*, vol. 7, no. 67, p. eabm7187, 2022.

[6] M. J. Yang, H. Chung, Y. Kim, K. Park, and J. Kim, "A body-scale robotic skin using distributed multimodal sensing modules: Design, evaluation, and application," *IEEE Transactions on Robotics*, vol. 41, pp. 96–109, 2025.

[7] W. Zheng, D. Guo, W. Yang, and H. Liu, "A large-area robotic skin for intelligent tactile interaction of collaborative robots," *IEEE/ASME Transactions on Mechatronics*, 2025.

[8] H. Chen, X. Yang, P. Wang, J. Geng, G. Ma, and X. Wang, "A large-area flexible tactile sensor for multi-touch and force detection using electrical impedance tomography," *IEEE Sensors Journal*, vol. 22, no. 7, pp. 7119–7129, 2022.

[9] C. Kohlbrenner, C. Escobedo, S. S. Bae, A. Dickhans, and A. Roncone, "Gentact toolbox: A computational design pipeline to procedurally generate context-driven 3d printed whole-body artificial skins," in *2025 IEEE International Conference on Robotics and Automation (ICRA)*. IEEE, 2025, pp. 4716–4722.

[10] C. Kohlbrenner, A. Soukhovei, C. Escobedo, N. Nechyporenko, and A. Roncone, "Design, mapping, and contact anticipation with 3d-printed whole-body tactile and proximity sensors," *arXiv preprint arXiv:2412.00672*, 2026.

[11] Y. Huang, D. Hardman, C. Bascucci, F. Clemens, and T. G. Thuruthel, "Design and modelling of electrical impedance tomography-based 3d-printed patterned soft tactile skins," in *2025 IEEE 8th International Conference on Soft Robotics (RoboSoft)*. IEEE, 2025, pp. 1–6.

[12] H. Chen, Z. Wang, K. Langlois, P. Mohamadi, H. Tian, T. Verstraten, and B. Vanderborght, "Investigating a novel 3D-printed electrical impedance tomography sensor for monitoring the interaction pressure on a customized physical interface in wearable robots," vol. 257, p. 118714.

[13] Recreus, "Conductive filaflex - electrically conductive TPU filament," [Online], 2018, technical Data Sheet. Available: https://filament2print.com/en/index.php?controller=attachment&id_attachment=756.

[14] ——, "Filaflex 60a — flexible TPU filament," [Online], 2024, product and technical information. Available: https://recreus.com/en/products/filaflex-60a?variant=45921624424707.

[15] A. Adler and R. Guardo, "Electrical impedance tomography: regularized imaging and contrast detection," *IEEE transactions on medical imaging*, vol. 15, no. 2, pp. 170–179, 1996.

[16] A. Adler and W. R. Lionheart, "Uses and abuses of eidors: an extensible software base for eit," *Physiological measurement*, vol. 27, no. 5, pp. S25–S42, 2006.